A 3D Laplacian-Driven Parametric Deformable Model

Tian Shen[1,2] Xiaolei Huang[1] Hongsheng Li[1] Edward Kim[1]
Shaoting Zhang[3] Junzhou Huang[4]

[1] Department of Computer Science and Engineering, Lehigh University, USA
[2] Corporate Technology, Siemens Ltd., China
[3] Department of Computer Science, Rutgers University, Piscataway, USA
[4] Department of Computer Science and Engineering, University of Texas at Arlington, USA

Abstract

3D parametric deformable models have been used to extract volumetric object boundaries and they generate smooth boundary surfaces as results. However, in some segmentation cases, such as cerebral cortex with complex folds and creases, and human lung with high curvature boundary, parametric deformable models often suffer from over-smoothing or decreased mesh quality during model deformation. To address this problem, we propose a 3D Laplacian-driven parametric deformable model with a new internal force. Derived from a Mesh Laplacian, the internal force exerted on each control vertex can be decomposed into two orthogonal vectors based on the vertex's tangential plane. We then introduce a weighting function to control the contributions of the two vectors based on the model mesh's geometry. Deforming the new model is solving a linear system, so the new model can converge very efficiently. To validate the model's performance, we tested our method on various segmentation cases and compared our model with Finite Element and Level Set deformable models.

1. Introduction

Deformable models have been used extensively in image segmentation. According to their representation and implementation, they can be classified as either parametric (explicit) or geometric (implicit) deformable models. Parametric deformable models, with *Snakes* [5] as a representative, represent the model boundary parametrically using spline curves or parametric surfaces. They have associated internal smoothness forces and are also influenced by external image forces. Using 3D parametric models [10] for segmenting objects in medical image volumes has the advantages of directly extracting a smooth boundary surface and guaranteeing coherence between images slices. The main concern with 3D parametric models is the computational cost due to a large number of variables. Thus Finite Element Method (FEM) based parametric deformable models are widely used [2], [18], [17]. Using FEM, the model is represented as a continuous surface in the form of weighted sums of local polynomial basis functions. By encoding the spatial information and connectivity about the vertices into the *stiffness matrix*, deformation of the model is solved through a linear system, which is efficient. Because the internal forces keep the model surface smooth, on one hand, FEM models have been shown to achieve good results in segmenting objects with smooth boundary such as the left ventricle [17]; on the other hand, these models often have difficulty delineating the boundary of objects with complex folds and creases, or high curvature regions.

The other class of deformable models is level set based geometric models [9], [19]. This approach represents a curve or a surface implicitly as the zero level set of a higher-dimensional scalar function (level set function). And level set models deform based on the theory of curve evolution with their speed function specifically designed to incorporate image gradient information. Geometric deformable models have been adopted with considerable success for image segmentation since they are parametrization-free and can be easily extended from 2D to 3D. Their topology flexibility also allows the extraction of multiple objects simultaneously. The topology-freedom is not always desirable, however. For instance, a fixed-topology model may be more suitable when the object of interest is specified and its topology is known [18]. Thus, topology-preserving level set methods have been proposed [4], [16], in which tests are conducted and steps are taken to process the computed level set functions to prevent undesirable topology changes.

In this paper, we consider the problem of segmenting a specific object with known topology in 3D. Both parametric deformable models and topology-preserving level set models are applicable. While parametric models directly extract object surfaces represented by triangular meshes, traditional FEM models suffer from over-smoothing and can not

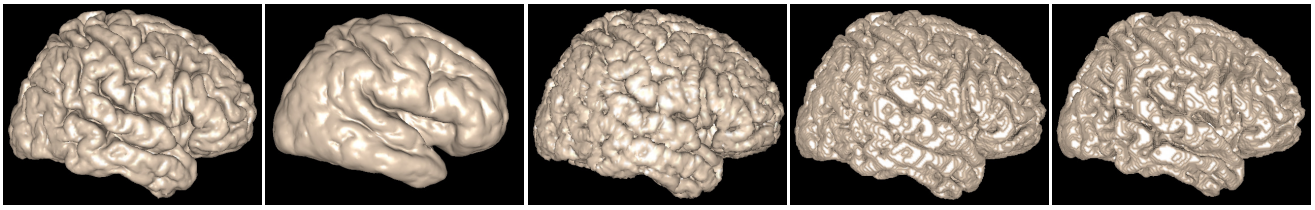

(a) (b) (c) (d) (e)

Figure 1. Cerebral cortex segmentation on simulated MRI images provided by BrainWeb (http://www.bic.mni.mcgill.ca/brainweb/). The external forces of (a), (b) and (c) are defined in (23). The internal forces of (b) and (c) are based on the *stiffness matrix* A in (2). (a) The result of our method, (b) the result of a traditional FEM based 3D deformable model, (c) the result of the FEM based model with weaker internal force, (d) the result of the Active Contour Without Edges [1] after surface reconstruction, and (e) the result of Distance Regularized Level Set Evolution [6] after surface reconstruction.

give satisfactory results when segmenting objects with complex surface structure or high curvature regions. Topology-preserving level set, on the other hand, will require extra processing steps to reconstruct the boundary surface from its binary map result, and to prevent change of topology. We propose a new method that modifies the internal forces exerted on a *non-FEM* parametric deformable model in order to overcome over-smoothing and directly extract object boundary as a high-quality triangular mesh.

The proposed new model is represented as a simplex mesh. Its internal forces are derived from the mesh Laplacian, which is widely used in mesh shape optimization and editing [13], [21]. By decomposing the Laplacian of each vertex into two orthogonal vectors—one on and another perpendicular to the vertex's tangential plane, we observe that (i) the tangential vector is always desirable in preserving mesh quality, (ii) the perpendicular vector has double effects—on the positive side, it helps overcome local minima caused by noise in images during segmentation, and on the negative side, it is found to cause the mesh's over-smoothing problem. The new 3D deformable model we introduce has internal forces that keep fully the vector projected onto the tangential plane since it helps maintain mesh quality. The contribution of the other vector perpendicular to the tangential plane is automatically adjusted through a weighting function defined based on current mesh quality. We demonstrate that, on segmenting objects with complex or high-curvature boundary surfaces such as the brain cerebral cortex (Figure 1) or lung (Figure 6), our method achieves better segmentation results than traditional FEM based 3D deformable model and level set methods [1], [6], in terms of accuracy and quality of the resulting boundary surface mesh. Furthermore, the new model can still deform efficiently since model deformation is derived by solving a linear system in which the matrix is very sparse.

2. Background

In this section, we briefly review the mathematical definition of traditional FEM based deformable models using a continuous piecewise-linear basis function[1]. We analyze the internal forces on these models to discuss the cause of the over-smoothing problem.

2.1. 3D FEM based Deformable Models

A 3D FEM deformable model is an elastic surface discretized as a simplex mesh (or finite element triangulation), which can deform under the influence of internal smoothness forces and external image forces derived from the model's energy function. The mesh Λ is represented as a graph $\mathbf{G} = (\mathbf{V}, \mathbf{E})$, with vertices $\mathbf{V}$ and edges $\mathbf{E}$. Given the basis function ϕ_i of the ith vertex $\mathbf{v}_i$ and the number of vertices $n = |\mathbf{V}|$, the deformable model is represented by $\Lambda(\mathbf{x}) = \sum_{i=1}^{n} \phi_i(\mathbf{x})\mathbf{v}_i$, in which $\mathbf{x} \in \mathbf{R}^3$. And the basis function $\phi_i(\mathbf{v}_j)$ is defined as

$$\phi_i(\mathbf{v}_j) = \begin{cases} 1 & i = j, \\ 0 & i \neq j, \end{cases} \tag{1}$$

where ϕ_i is a continuous piecewise linear function, and $\mathbf{v}_i$ and $\mathbf{v}_j$ are the ith and jth vertices of the model.

Given the external force vector $F_V^{ext} = [f_1^{ext}, f_2^{ext}, ..., f_n^{ext}]^T$, minimizing the energy function is done by solving

$$AV = F_V^{ext}, \tag{2}$$

where matrix A is the *stiffness matrix* [8], whose size is $n \times n$. $V = [\mathbf{v}_1, \mathbf{v}_2, ..., \mathbf{v}_n]^T$ is the vector of control vertices on the surface. More specifically, the ith row and jth column element of A, a_{ij}, is defined as

$$a_{ij} = \begin{cases} \int_\Lambda (\nabla\phi_i \cdot \nabla\phi_j) d\Lambda & i = j \text{ or } (i,j) \in \mathbf{E} \\ 0 & \text{otherwise} \end{cases}. \tag{3}$$

Using finite differences in time, the model can deform iteratively [2]. (2) is optimized as:

$$(V^{(t)} - V^{(t-1)})/\tau + AV^{(t)} = F_{V^{(t-1)}}^{ext}, \tag{4}$$

[1] We use *FEM based 3D deformable models* to refer to *FEM based 3D deformable models using a continuous piecewise-linear basis function*.

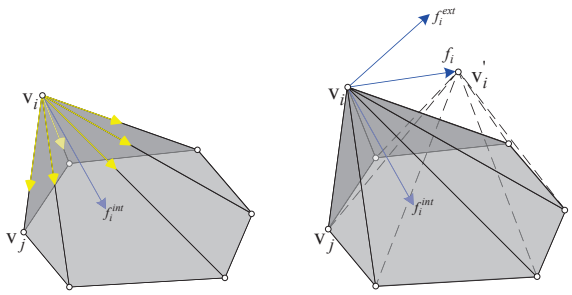

(a) (b)

Figure 2. (a) The internal force f_i^{int} of $\mathbf{v}_i$ is represented as a summation of a set of vectors pointing from the vertex to all its neighboring vertices, and (b) the vertex deforms according to the summation of internal force vector f_i^{int} and external force vector f_i^{ext}.

where $V^{(t)}$ is the vector of the model's vertices at the t-th iteration, and τ is the time step size. (4) can be written in a finite differences formulation, as

$$\begin{aligned} &MV^{(t)} = V^{(t-1)} + \tau F^{ext}_{V^{(t-1)}}, \\ &M = (I + \tau A). \end{aligned} \tag{5}$$

Based on the basis function in (1), since each vertex in the simplex model is only connected to a small number of vertices, M is a sparse and positive definite matrix. The solution of (5) can be obtained very efficiently.

2.2. Analysis of the Conventional Internal Force

(4) can be further reformulated according to the internal and external forces

$$V^{(t)} = V^{(t-1)} + \tau(F^{int} + F^{ext}_{V^{(t-1)}}), \tag{6}$$

where

$$F^{int} = -AV^{(t)}, \tag{7}$$

so the ith element f_i^{int} in F^{int} represents the internal force on the ith vertex.

The internal force on the ith vertex $\mathbf{v}_i$ is defined based on (7)

$$f_i^{int} = -(a_{ii}\mathbf{v}_i + \sum_{(i,j)\in\mathbf{E}} a_{ij}\mathbf{v}_j). \tag{8}$$

Since the *stiffness matrix* A also has the property

$$a_{ii} + \sum_{(i,j)\in\mathbf{E}} a_{ij} = 0, \quad \text{for any } \mathbf{v}_i \in \mathbf{V}, \tag{9}$$

then (8) can be written as

$$f_i^{int} = \sum_{(i,j)\in\mathbf{E}} a_{ij}(\mathbf{v}_i - \mathbf{v}_j). \tag{10}$$

As shown in Figure 2.(a), the internal force on the ith vertex, f_i^{int}, is a summation of a set of vectors which are pointing from the ith vertex to its neighboring vertices. When applying the deformable model to segment an object, the control vertex moves according to the summation of its internal force vector and the external force vector, as shown in Figure 2.(b). In the final converged result, the summation of internal and external force vectors of each vertex is approximately equal to zero.

The internal force vectors of the FEM model keep the model's surface smooth and also help it overcome the negative effects of image noise. However, if the target object has a complex surface (*e.g.*, the cerebral cortex in Figure 1) or contains high curvature boundary (*e.g.*, the bottom of the lung in Figure 6), the internal force vectors might cause the surface to be over-smoothed and thus have vertices deviate away from desired object boundaries.

To alleviate this problem, one may decrease the weight of the internal force to make the external force have more power in controlling the model's deformation, by utilizing an automatic parameter adjustment technique [12] or by receiving parameter adjustment input from an experienced user. Often, to allow the model to fit the details on object boundary, parameter adjustment involves lowering the weight of the internal force and decreasing the model-deformation step size. However, such adjustment would decrease the model mesh's quality and increase the number of iterations necessary for the model to converge. A solution to restore the mesh quality is to adopt *Remeshing with Detail Preserving* methods [7], [13]. Remeshing can be applied to the model mesh after every few iterations. But typical remeshing techniques are time-consuming. Further, when the internal force is made weaker, the model may suffer from a sharp degeneration in mesh quality due to strong external forces pulling the model in different directions as well as effects of image noise. It is likely that the mesh quality would become too poor to be recovered, causing difficulty in remeshing and leading to poor segmentation results.

3. Methodology

We present a new 3D deformable model derived from the mesh Laplacian, with the objective of achieving efficient detail-preserving segmentation while maintaining high model-mesh quality.

3.1. The Novel Internal Force

3.1.1 Mesh Laplacian

The new *Laplacian-driven parametric deformable model* we propose is still represented as a simplex mesh, but it has a novel internal force definition derived from the mesh Laplacian [13]. For the ith vertex $\mathbf{v}_i$, the uniformly weighted Laplacian δ_i is

$$\delta_i = \sum_{(i,j)\in\mathbf{E}} \mathbf{v}_j - \mathbf{w}_i\mathbf{v}_i = \sum_{(i,j)\in\mathbf{E}} (\mathbf{v}_j - \mathbf{v}_i), \tag{11}$$

where $\mathbf{w}_i$ is the number of vertices connected with $\mathbf{v}_i$.

Given the number of vertices n, the element $\mathbf{l}_{ij}$in the $n \times n$ Laplacian matrix $\mathbf{L}$ is represented as

$$\mathbf{l}_{ij} = \begin{cases} \mathbf{w}_i & i = j, \\ -1 & (i,j) \in \mathbf{E}, \\ 0 & \text{otherwise.} \end{cases} \quad (12)$$

In Figure 3.(a), the Laplacian of the ith vertex is shown as the blue arrow. Serving as the internal force, the Laplacian moves the ith vertex to the centroid of its neighboring vertices. This procedure can be decomposed into two substeps. Firstly, $\mathbf{v}_i$ is moved on its tangential plane in favor of having triangles with equal areas. Secondly, $\mathbf{v}_i$ is further moved along its normal direction to reach the centroid. According to these two steps, δ_i can be decomposed into two vectors associated with the vertex's tangential plane, which are the red vector δ_i^{tang} on the tangential plane and the green vector δ_i^{perp} perpendicular to the tangential plane, as shown in Figure 3.(b). δ_i^{tang} has the desired effect of balancing the areas of neighboring triangles (Figure 3.(c)), and δ_i^{perp} moves the vertex along the normal direction which shrinks the model and makes it a smooth surface. When segmenting objects with complex surfaces, the above mentioned over-smoothing problem is caused by δ^{perp}. If simply decreasing the influence of the internal force, the weight of δ^{tang} is also reduced, which may severely affect the mesh quality (Figure 1.(c)). In our method, by decomposing the internal force into two vectors, the over-smoothing problem can be solved as keeping the contribution of δ_i^{tang} and lowering the influence of δ_i^{perp} (Figure 1.(a)).

The decomposition of internal forces has been used on 2D parametric deformable contours in [3]. Based on a control vertex's tangential vector, the method [3] decomposed the internal force on the 2D parametric contour into two parts so as to automatically control the distances between neighboring vertices and the total number of control vertices. This method can not be extended to 3D, however, since 3D models have much more complex geometry and shape representation than 2D models. In 3D, the internal force vector of a control vertex in the traditional FEM based deformable model could also be decomposed into two vectors associated with the tangential plane of the vertex. We did not follow this approach because the *stiffness matrix* of the FEM model has the property of reducing the mobility of vertices [8], thus the internal force vector projected on the tangential plane vanishes, unable to effectively preserve mesh quality. Furthermore, the *stiffness matrix* in an FEM model needs to be updated after each iteration since it depends on the spatial positions of the connected vertices. In contrast, the Laplacian matrix used by our model has the property that its weights do not depend on the vertex position, thus the weights only need to be calculated once and can be precomputed after the model is initialized. Therefore, we prefer the mesh Laplacian over FEM.

3.1.2 Internal Forces Based on Mesh Laplacian

δ_i^{prep} in Figure 3.(b) can be calculated based on:

$$\delta_i^{perp} = (\widehat{\mathbf{n}}_i \cdot \delta_i)\widehat{\mathbf{n}}_i. \quad (13)$$

where $\widehat{\mathbf{n}}_i$ is the normal of $\mathbf{v}_i$. In this paper, we define it as the average of the normals of the vertex's adjacent surfaces.

Then δ_i^{tang} in the tangential plane is

$$\delta_i^{tang} = \delta_i - \delta_i^{perp} = \sum_{(i,j)\in\mathbf{E}} \mathbf{v}_j - \mathbf{w}_i\mathbf{v}_i - \delta_i^{perp}. \quad (14)$$

Using (14) as the new internal force and applying finite differences, the deformation equation for the ith vertex is

$$\mathbf{v}_i^{(t)} + \tau(\mathbf{w}_i\mathbf{v}_i^{(t)} - \sum_{(i,j)\in\mathbf{E}} \mathbf{v}_j^{(t)} + (\delta_i^{perp})^{(t)}) = \mathbf{v}_i^{(t-1)} + \tau f_i^{ext}, \quad (15)$$

where τ is the step size, $\mathbf{v}_i^{(t)}$ is the ith vertex's location at the t-th iteration. In (15), the unknown parameters are $\mathbf{v}_i^{(t)}$, $\mathbf{v}_j^{(t)}$ and $(\delta_i^{perp})^{(t)}$. Since we use finite differences, we assume the shape of the model does not change significantly in each iteration, so we approximate $(\delta_i^{perp})^{(t)}$ with $(\delta_i^{perp})^{(t-1)}$, *i.e.*,

$$(\delta_i^{perp})^{(t)} = (\delta_i^{perp})^{(t-1)}, \quad (16)$$

where $(\delta_i^{perp})^{(t-1)}$ can be obtained from the current mesh's geometric shape directly. We then have

$$\mathbf{v}_i^{(t)} + \tau(\mathbf{w}_i\mathbf{v}_i^{(t)} - \sum_{(i,j)\in\mathbf{E}} \mathbf{v}_j^{(t)} + (\delta_i^{perp})^{(t-1)}) = \mathbf{v}_i^{(t-1)} + \tau f_i^{ext}. \quad (17)$$

When the ith vertex moves according to (17), the new internal force δ_i^{tang} moves the vertex only on its tangential plane without shrinking the model, which overcomes the over-smoothing problem and keeps the mesh quality effectively. However, testing the model on 3D medical images, we find the model becomes more sensitive to noise. The reason is that the vector perpendicular to the tangential plane δ^{perp} has the property of helping the vertex pass some local minima caused by noise and stop at strong boundaries. And δ^{perp} also has positive effects on improving mesh quality, since moving the vertex along its normal direction also reduces the areas of its neighboring triangles and make them more similar to an equilateral triangle. To keep the benefits of δ^{perp}, we adopt a weighting function $\omega(\mathbf{v})$ to control its contribution. The internal force is thus redefined as:

$$f_i^{int} = \sum_{(i,j)\in\mathbf{E}} \mathbf{v}_j - \mathbf{w}_i\mathbf{v}_i - \omega(\mathbf{v}_i)\delta_i^{perp}. \quad (18)$$

To define $\omega(\mathbf{v})$, we use the vertex's neighboring triangle's *radius ratio* ϵ [14], which is mapped to $[0, 1]$ as

$$\epsilon = 2\frac{r_{ins}}{R_{cir}}, \quad (19)$$

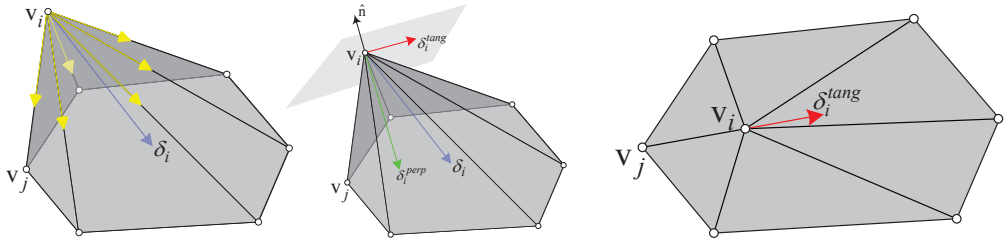

(a) (b) (c)

Figure 3. Illustration of the novel internal force. (a) The internal force vector of the vertex is shown in the neighboring triangles, (b) given the vertex's normal direction, the internal force vector can be decomposed into two vectors according to the vertex's tangential plane, and (c) v_i moves on the tangential plane in favor of having triangles with equal areas.

where r_{ins} and R_{cir} are the radii of the inscribed and circumscribed circles of the triangle. $\epsilon = 1$ indicates a well shaped equilateral triangle and $\epsilon = 0$ means a degenerated triangle. The *radius ratio* of the ith vertex $r(\mathbf{v}_i)$ is defined as the average *radius ratio* of all its neighboring triangles. A high $r(\mathbf{v})$ means the vertex's neighboring triangles are in good shape and $\omega(\mathbf{v})$ is set as close as possible to 1. Then the internal force vector can be mapped onto the tangential plane to make sure the vertex deforms without shrinking. Once $r(\mathbf{v})$ decreases because of noise or some other factors, we assign $\omega(\mathbf{v})$ a relatively small value. Then δ^{perp} is partially preserved to reduce the effect of noise and to restore the neighboring triangles of the vertex to a good shape.

In this paper, we introduce two ways to set $\omega(\mathbf{v})$ based on the *radius ratio*. We first define $\omega(\mathbf{v})$ as a Fermi function (sigmoidal), which is

$$\omega(\mathbf{v}) = \frac{1}{1 + e^{-s(r(\mathbf{v})-\mu)}}, \tag{20}$$

where s is the steepness, and μ controls the overall mesh quality level. s and μ are empirically set as 20 and 0.7.

Secondly, taking the relative frequency of *radius ratio* into account, we adopt its cumulative density function (CDF) to map from $r(\mathbf{v})$ to weight $[0, 1]$. In this way, the weighting function is defined as a normalized discrete summation over $r(\mathbf{v})$ for all the vertices:

$$\omega(\mathbf{v}_i) = \sum_{\mathbf{v}_k \in \mathbf{V}} c_{ik},$$
$$c_{ik} = \begin{cases} \frac{1}{|\mathbf{V}|} & r(\mathbf{v}_k) \le r(\mathbf{v}_i) \\ 0 & r(\mathbf{v}_k) > r(\mathbf{v}_i) \end{cases}. \tag{21}$$

Based on our experience, (20) is more suitable to segment objects with high curvature boundaries and (21) is more suitable to segment objects with complex surfaces.

Compared with (14), (18) has a weighting function ranging from 0 to 1, which is used to control the contribution of δ^{perp} in Figure 3. Considering all the control vertices, the linear system for the new deformable model is defined based on (14) as

$$M' \begin{bmatrix} V^{(t)} \\ D^{(t)} \end{bmatrix} = \begin{bmatrix} V^{(t-1)} \\ D^{(t-1)} \end{bmatrix} + \tau \begin{bmatrix} F^{ext}_{V^{(t-1)}} \\ 0 \end{bmatrix},$$
$$M' = \begin{bmatrix} M_{00} & M_{01} \\ 0 & M_{11} \end{bmatrix} = (I + \tau \begin{bmatrix} L_{00} & L_{01} \\ 0 & 0 \end{bmatrix}), \tag{22}$$

where L_{00} is the $n \times n$ Laplacian matrix in (12), L_{01} is a $n \times n$ diagonal matrix derived from the weighting function $\omega(\mathbf{v})$ to control the weights of δ^{perp}. $D^{(t)}$ and $D^{(t-1)}$ are the $n \times 1$ vectors encoding δ^{perp} of all the vertices at time t and $t-1$ respectively. M_{11} is the identity matrix of size n. The size of M' is $2n \times 2n$, and it is very sparse. Solving (22) is still very efficient. In 3D, (22) is solved three times, for the x, y and z components separately.

4. Experiments

In this section, we show experiments that test our new model. We also compare its performance with several other deformable models: an FEM model (Section 2.1) with normal or weak internal forces, and two level set based algorithms—Active Contour Without Edges (ACWE) [1] and Distance Regularized Level Set Evolution (DRLSE) [6]. During comparison, all models use the same initialization. The test datasets include a 3D volume of a synthetic object whose boundary has high curvature regions (Figure 4), a 3D simulated MRI brain image from BrainWeb (Figure 1), and 10 human lung volumetric datasets from the NCI Lung Image Database Consortium (LIDC) (Figure 6). The parameter settings for the various models and the models' performance measures are summarized in Table 1.

4.1. Experimental Setup

On the 3D synthetic dataset and the lung datasets, we compared our model with the FEM model. Both models are initialized in the same way, *i.e.*, spheres or ellipsoids near the object with user-specified radii. To segment the cerebral cortex from the MRI brain image, we compared our model

with the FEM model with normal internal forces, the FEM model with weakened internal forces, and the two level set based algorithms ACWE and DRLSE; all models use the same initialization which is the pre-segmented brain White Matter obtained by [20]. For our proposed parametric deformable model with Laplacian-driven internal forces, we used (20) to control the weight of δ^{perp} when segmenting the synthetic object and human lungs, and used (21) for segmentation of the brain cerebral cortex.

To focus on evaluating only the performance of the new Laplacian-driven internal force, in the experiments, we used the same external force to deform our model and the FEM based model. Similar to *T-Snakes* [11], the external force is set according to the intensity values and the vertices' normals. For the ith vertex, it is

$$f_i^{ext} = \begin{cases} \gamma \widehat{\mathbf{n}}_i & I(\mathbf{v}_i) \geq T, \\ -\gamma \widehat{\mathbf{n}}_i & \text{otherwise}, \end{cases} \tag{23}$$

where $\widehat{\mathbf{n}}_i$ is the normal of the vertex, $I(\mathbf{v}_i)$ denotes the intensity value of the ith vertex, and T is the mean intensity value of the image volume.

The settings of step size τ and the weight of external force γ for our model and the FEM models are shown in Table 1. Note that our model did not need parameter tuning and used the same parameter setting for all experiments. In contrast, the FEM model needs different parameter settings for different segmentation tasks, and in the experiments, we manually set the FEM model' parameters to enable it to grow as much as possible under the influence of strong external forces toward object boundary. The convergence criterion for our model and the FEM model is defined based on the model vertices' movements: we assume the model reaches the final converged result if all the vertices move less than a maximum of two voxels in a certain iteration. For the two level set methods used in Figure 1.(d)–(e), we empirically set their parameters to make the models achieve their best segmentation results.

To illustrate the models' performance, we calculated the Dice Similarity Coefficient (DSC) [15] values to measure the segmentation accuracy and used the *radius ratio* of mesh triangles to measure the mesh quality, see Table 1.

4.2. Experimental Results

Figure 4 shows segmentation results on the 3D synthetic dataset. From the final results viewed in 3D and 2D cross-sectional planes, one can clearly see that our model precisely found the object boundary but the conventional FEM based model generated a smooth surface that did not fit well at corners on the boundary. The mean *radius ratio* values of the resulting boundary surface meshes by our model and the FEM model are 98.87% and 97.91%, respectively.

Figure 1 compares the cerebral cortex segmentation results using our method, the FEM model with normal internal forces, the FEM model with weakened internal forces,

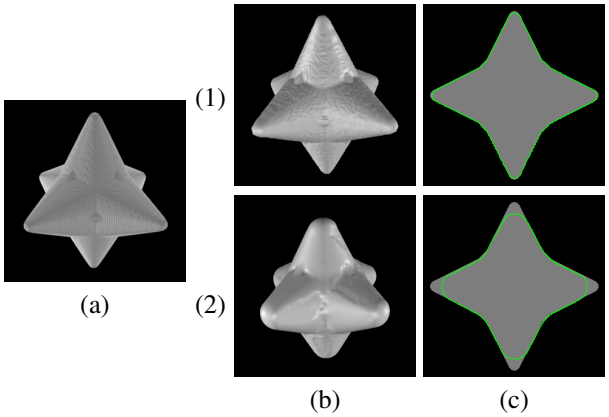

Figure 4. Segmentation results on a 3D synthetic dataset. (a) Volume rendering of the dataset, (b) the segmentation results viewed in 3D, (c) the segmentation results viewed in 2D cross-sectional planes, (1) the result of our method, and (2) the result of the FEM based method.

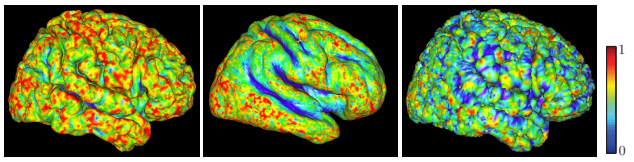

Figure 5. Visualization of mesh quality evaluation by color-mapping the result meshes' *radius ratio* values using the cumulative density function of the result in Figure 1.(c). (a) Result of our method in Figure 1.(a), (b) result of the FEM model with normal smoothness constraints in Figure 1.(b), (c) result of the FEM model with weakened smoothness constraints in Figure 1.(c), and (d) the color bar.

the ACWE and DRLSE. For our model and the FEM models, the initialization is the iso-surface mesh reconstructed from the pre-segmented White Matter; for the two level set methods, the initialization is the signed distance transform of the White Matter. Our result is shown in Figure 1.(a), and has the highest mean *radius ratio* value 92.3%. In Figure 1.(b)–(c), FEM based models either became too smooth or had low mesh quality. The mean *radius ratio* values of Figure 1.(b)–(c) are 89.1% and 83.4%. With a relatively weak internal force, the FEM model had to adopt a small step size to deform, which increased the running time as shown in Table 1. In Figure 1.(d)–(e), a post-processing surface reconstruction step was necessary to obtain the boundary surface from level set's volumetric segmentation result, and the reconstructed surface has low mesh quality, affecting accuracy and visualization. The mean *radius ratio* values of Figure 1.(d)–(f) are 77.4% and 77.9%.

In Figure 5, we visualize the mesh quality comparison results of Figure 1.(a)–(c) by color-mapping the mesh triangles' *radius ratios* using the cumulative density function (CDF) defined in (21). Here we adopt the CDF of the mesh

Table 1. Parameter settings and quantitative evaluation of our method and other methods.

	Synthetic Data		Human Lung		Human Brain				
	Ours	FEM	Ours	FEM	Ours	Fig. 1.(b)	Fig. 1.(c)	Fig. 1.(d)	Fig. 1.(e)
τ (step size)	0.8	0.5	0.8	0.4	0.8	0.6	0.1	n/a	n/a
γ (weight of external force)	1	2	-1	-1.8	1	1.5	2	n/a	n/a
DSC	99.2%	95.3%	96.3%	93.2%	95.5%	88.7%	93.6%	94.6%	93.8%
Iterations	63	68	58	68	45	48	90	32	26
Running Time	79.4s	54.4s	70.1s	61.88s	43.4s	31.3s	71.6s	52.2s	39.6s

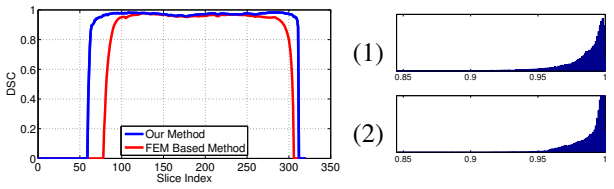

(a) (b)

Figure 7. DSC and mesh quality (*radius ratio*) evaluation of the segmentation results in Figure 6.(a). (a) DSC results of different axial slices, (b) the vertices' *radius ratio* distribution, (1) *radius ratio* distribution of our method, and (2) *radius ratio* distribution of the FEM based method. The left and right lungs extend from the 53rd slice to the 314th slice.

in Figure 1.(c). Our result contains the most red regions, indicating it has the best mesh quality.

We also evaluated our method on 10 human lung datasets and show 4 of them in Figure 6. From the DSC values shown in Table 1, our model produced a noticeable improvement in accuracy compared to the FEM model. In Figure 7, we plotted the DSC value in each axial slice (0 means there is no segmentation result in that slice) and showed the distribution of the model vertices' *radius ratio* from the dataset in Figure 6.(a). Since the objects extend from the 53rd slice to the 314th slice, from the figure we can see that our method correctly recovered the objects with high DSC value in each slice, while the FEM model missed parts of the objects in the top and bottom slices. Both our model and the FEM model produced high-quality 3D surface meshes, with mean *radius ratio* values above 97%. To further demonstrate the results, we show 4 sets of comparison results from different cross-sectional planes in Figure 8.

5. Conclusion and Future Work

In this paper, we proposed a new 3D Laplacian-driven deformable model based on mesh Laplacian aiming to segment with better accuracy objects that have complex surfaces or high curvature boundaries. The main contributions include: (1) decomposing the internal force of each vertex into two vectors according to the vertex's tangential plane, the 3D parametric deformable model's internal force can be considered as consisting of two separated parts; (2) maintaining the vector projected onto the tangential plane and using a mesh-geometry based weighting function to control the contribution of the vector perpendicular to the tangential plane, the model can thus be used to segment objects with complex surface or high curvature regions, while preserving the mesh quality; (3) deforming the new model is equivalent to getting the solution of a linear system, which is very efficient. Testing the new model on 3D synthetic, human lung and brain datasets and comparing with other parametric and geometric deformable models, our model achieved better performance with little sensitivity to parameter settings.

Acknowledgements.

This research was supported in part by the NSF grant IIS-0812120 and NIH grant R21GM083928.

References

[1] T. Chan and L. Vese. Active contours without edges. *IEEE Trans. Image Processing*, 10:266–277, 2001.

[2] L. Cohen and I. Cohen. Finite-element methods for active contour models and balloons for 2-D and 3-D images. *IEEE Trans. Pattern Analysis and Machine Intelligence*, 15:1131–1147, 1993.

[3] H. Delingette and J. Montagnat. Shape and topology constraints on parametric active contours. *Computer Vision and Image Understanding*, 83:140–171, 2001.

[4] X. Han, C. Xu, and J. Prince. A topology preserving level set method for geometric deformable models. *IEEE Trans. Pattern Analysis and Machine Intelligence*, 25:755–768, 2003.

[5] M. Kass, A. Witkin, and D. Terzopoulos. Snakes: Active contour models. *International Journal of Computer Vision*, 1:321–331, 1988.

[6] C. Li, C. Xu, C. Gui, and M. Fox. Distance regularized level set evolution and its application to image segmentation. *IEEE Trans. Image Processing*, 19:3243–3254, 2010.

[7] Y. Liu, W. Wang, B. Lévy, F. Sun, D. Yan, L. Lu, and C. Yang. On centroidal voronoi tessellation–energy smoothness and fast computation. *ACM Trans. Graphics*, 28:1–17, 2009.

[8] D. Logan. *A First Course in the Finite Element Method*. CL Engineering, 2006.

[9] R. Malladi, J. Sethian, and B. Vemuri. Shape modeling with front propagation: A level set approach. *IEEE Trans. Pattern Analysis and Machine Intelligence*, 17:158–175, 1995.

[10] T. McInerney and D. Terzopoulos. Deformable models in medical image analysis: A survey. *Medical Image Analysis*, 1:91–108, 1996.

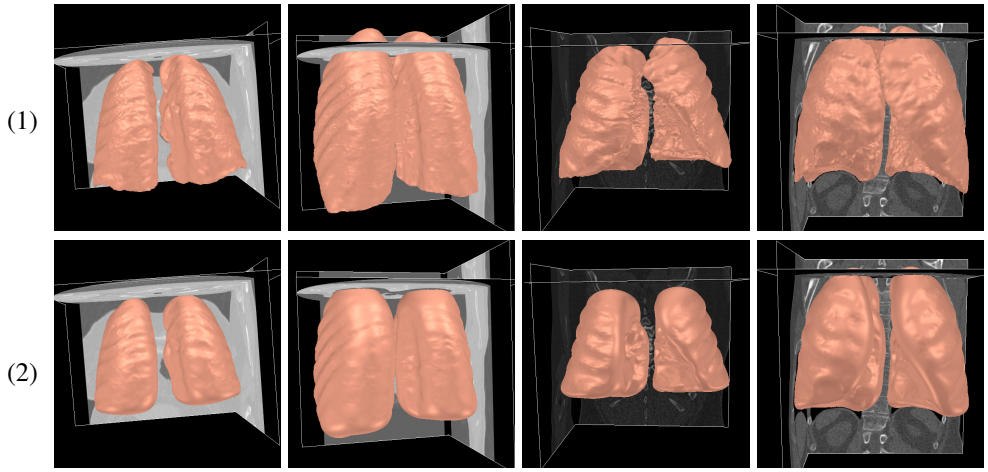

Figure 6. Segmentation results on 4 human lung datasets, (1) the results of our method, (2) the results of the conventional FEM based method, and (a-d) 4 different image volumes from the human lung datasets.

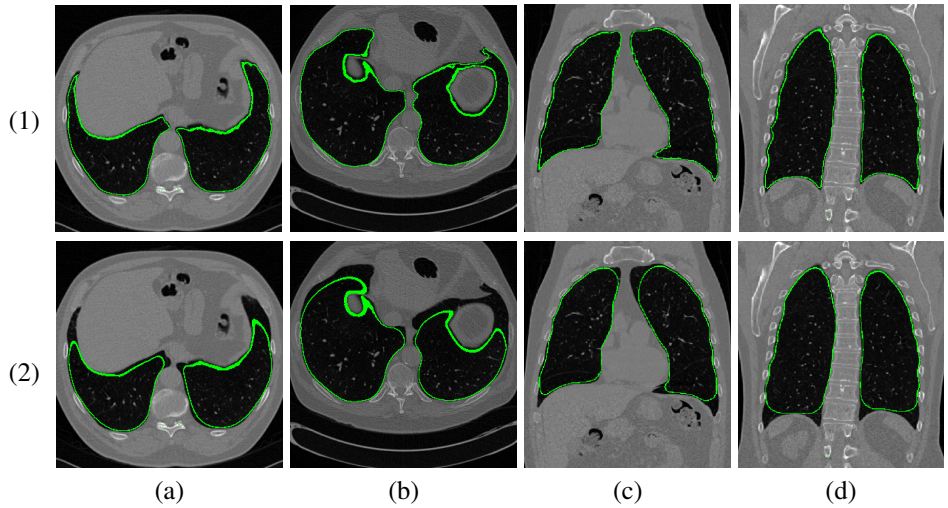

Figure 8. Lung segmentation results in Figure 6 viewed from 4 different sample cross-sectional planes. (1) The result of our method and (2) the result of the conventional FEM based method.

[11] T. McInerney and D. Terzopoulos. T-snake: Topology adaptive snakes. *Medical Image Analysis*, 4:73–91, 2000.

[12] D. Metaxas and I. Kakadiaris. Elastically adaptive deformable models. *IEEE Trans. Pattern Analysis and Machine Intelligence*, 24:1310–1321, 2002.

[13] A. Nealen, O. Sorkine, M. Alexa, and D. Cohen-Or. A sketch-based interface for detail-preserving mesh editing. *Proc. SIGGRAPH*, pages 1142–1147, 2005.

[14] P. Pébay and T. Baker. Analysis of triangle quality measures. *Mathematics of Computation*, 72:1817–1839, 2003.

[15] A. Popovic, M. de la Fuente, M. Engelhardt, and K. Radermacher. Statistical validation metric for accuracy assessment in medical image segmentation. *Int'l Journal of Computer Assisted Radiology and Surgery*, 2:169–181, 2007.

[16] F. Ségonne. Active contour under topology control – genus preserving level sets. *International Journal of Computer Vision*, 79:107–117, 2008.

[17] T. Shen, H. Li, Z. Qian, and X. Huang. Active volume models for 3D medical image segmentation. *Proc. CVPR*, 2009.

[18] L. Staib and J. Duncan. Model-based deformable surface finding for medical images. *IEEE Trans. Medical Imaging*, 15:720–731, 1996.

[19] G. Sundaramoorthi, A. Yezzi, and A. Mennucci. Sobolev active contours. *International Journal of Computer Vision*, 73:345–366, 2007.

[20] C. Xu, D. Pham, M. Rettmann, D. Yu, and J. Prince. Reconstruction of the human cerebral cortex from magnetic resonance images. *IEEE Trans. Medical Imaging*, 18:467–480, 1999.

[21] S. Zhang, J. Huang, and D. Metaxas. Robust mesh editing using laplacian coordinates. *Graphical Models*, 73:10–19, 2011.